



Benzodifuroxazinones, a new class of heteroacene molecules for possible applications in organic electronics: Synthesis, electronic properties and crystal structure

Antonio Carella^{a,*}, Fabio Borbone^a, Antonio Roviello^a, Giuseppina Roviello^b, Angela Tuzi^a, Alexey Kravinsky^c, Rafi Shikler^{c,d}, Giovanni Cantele^e, Domenico Ninno^e

^a *Dipartimento di Chimica, Università degli Studi di Napoli "Federico II", Complesso Universitario Monte S. Angelo, Via Cintia snc, 80126 Napoli, Italy*

^b *Dipartimento per le Tecnologie, Università degli Studi di Napoli Parthenope, Centro Direzionale Isola C4, 80143 Napoli, Italy*

^c *Department of Electrical Computer Engineering, Ben-Gurion University of the Negev, POB 653 Beer-Sheva 84105, Israel*

^d *Ilse-Katz center for Nanotechnology, Ben-Gurion University of the Negev, POB 653 Beer-Sheva 84105, Israel*

^e *CNR-SPIN and Dipartimento di Scienze Fisiche, Università degli Studi di Napoli "Federico II", Complesso Universitario Monte S. Angelo, Via Cintia snc, 80126 Napoli, Italy*

ARTICLE INFO

Article history:

Received 31 October 2011

Received in revised form

28 March 2012

Accepted 31 March 2012

Available online 10 April 2012

Keywords:

Solid phase synthesis

Heteroacenes

Crystal structure determination

Density functional calc.

Organic electronics

Solid state fluorescence

ABSTRACT

A novel class of heteroacene molecules, benzodifuroxazin-4-ones, has been effectively synthesized by means of a thermally activated double cyclization reaction starting from amidic precursors. The new molecules were thermally and optically characterized, revealing an outstanding thermal stability to oxidation and an uncommon enhancement of fluorescent properties in solid state as compared to solution. As shown by single-crystal XRD analysis, the molecules crystallize in a face-to-face (π -stack) arrangement instead of the herringbone structure typical of the most acene derivatives. The electronic properties of both molecules and crystals have been investigated by means of a detailed Density Functional Theory computational analysis: very stable HOMO energies have been calculated and, from the band structure analysis, it is possible to suggest a preferential direction of charge transport along the π -stacking direction. All the reported properties indicate this new class of heteroacene derivatives as interesting candidates for a possible application in organic electronics.

© 2012 Elsevier Ltd. All rights reserved.

1. Introduction

Organic semiconductors has received a great deal of attention for their possible use as active layers in thin film electronic devices such as transistors [1–3], light emitting devices (OLED) [4–6] or solar cells [7–9]. As compared to the inorganic semiconductors typically used in electronics, the unique mechanical properties of organic molecules and polymers may allow the fabrication of flexible electronic devices, while their easier processability might open the way to low-cost manufacturing techniques such as spin-coating, ink-jet printing, and roll-to-roll printing processes [10]; this technological aspect is particularly striking in a field like electronics where manufacturing costs weight much more than the cost of the material itself. Another important factor justifying the huge interest in organic semiconductors is the possibility to design or modify π -conjugated chemical structures in ways that could directly impact the properties of the material.

Most of the investigated organic semiconductors could be roughly divided into two classes, conjugated polycyclic compounds with low molecular weight [11–15] and polyheterocycles [11,16,17]. As far as the former are concerned, oligoacenes are one of the most intensively investigated class of materials in the literature: organic transistors endowed with outstanding mobility have been fabricated by using pentacene and its derivatives as active layer. However, acene-type molecules show a number of drawbacks for practical applications like for instance a high-energy-lying HOMO and a narrow bandgap that make them extremely sensitive to photo-oxidation [18]. A possible synthetic approach for improving the oxidative stability is to insert, within the fused ring system, more electronegative heteroatoms [19,20].

The typical crystalline structure presented by heteroacene compounds is characterized by a herringbone pattern, in which the molecules are packed edge-to-face in 2D layers (with the highest charge mobility in this plane) [21]. However, theoretical works have shown that charge mobility in organic semiconductors is intrinsically related to the overlap of π molecular orbitals of adjacent conjugated molecules [22]; in this respect, the herringbone

* Corresponding author. Tel.: +39081674446; fax: +39081674367.

E-mail address: antonio.carella@unina.it (A. Carella).

structure is not the most suitable one and it could be argued that, in principle, higher mobility could be obtained by designing new molecules that crystallize in a face-to-face (π -stack) arrangement. Indeed, proper synthetic modifications of the molecules can turn the crystal packing from herringbone to π -stacked, for example through functionalization of the acene core with halogens [23,24] or bulky substituents in the peripositions of the oligoacenes [24,25].

In a recent paper dealing with the amino-benzodifurane reactivity, we hypothesized the formation of the **B-OXA** compound (see Fig. 1) based on an unprecedented penta-atomic fused heterocycle, a benzodifuroxazinone prepared through a cyclization reaction thermally initiated in the bulk [26]. While in the mentioned paper only preliminary results were reported, a later single-crystal X-Ray Diffraction (XRD) analysis confirmed the structure of the **B-OXA**.

Here, we report (for the first time) the optimized synthesis of **B-OXA** and of two new fluorinated derivatives, **FB-OXA** and **DFB-OXA**. The molecular structure of these molecules, presented in Fig. 1, shows several elements of interest: the core structure is composed of five fused rings, as in pentacene, and should allow a high degree of planarity that, in turn, could lead to high electrical performance. Moreover, because of the presence of more electronegative heteroatoms, it can be argued a higher stability of benzodifuroxazinone derivatives against oxidation, compared to that of pentacene. Finally, the versatility of the synthetic strategy to prepare this class of compounds could easily give access to a wide number of derivatives with tailored features.

The chemical physical properties of the three benzodifuroxazinones derivatives and their intermediates have been fully characterized. A peculiar feature of all three compounds is revealed in fluorescence experiments: they are good green emitters in solid state while they show very weak fluorescence when excited in solution. This phenomenon (also referred to in the literature as “aggregate induced emission, AIE” [27,28]) makes them interesting candidates in OLED technology.

The structures of **FB-OXA** and **DFB-OXA** have been resolved by means of single-crystal XRD. The obtained crystal structures and crystallographic coordinates have been used as the basis for a detailed computational analysis that will be extensively described in the next sections.

2. Materials and methods

2.1. Chemical and characterization

All solvents and reagent were purchased by Aldrich and used without further purification. The thermal behaviour of the compounds was studied by differential scanning calorimetry (Perkin–Elmer Pyris 1, nitrogen atmosphere, scanning rate 10 K/min), temperature controlled polarizing microscopy (Zeiss microscope, Mettler FP5 microfurnace) and thermo-gravimetric analysis

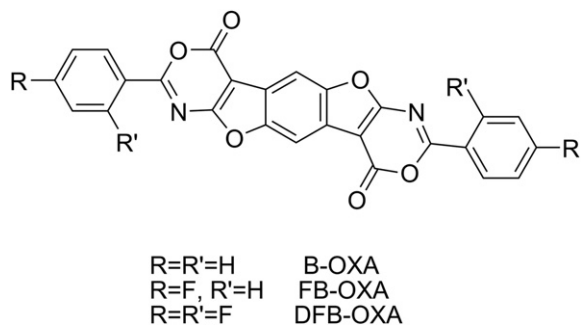


Fig. 1. Molecular structure of the prepared chromophores.

(TA SDT 2960, air, 20 K/min). ^1H and ^{13}C NMR spectra were recorded with a Varian XL 200-MHz apparatus. UV/Vis absorption and fluorescence spectra of the prepared chromophores, both in solution and as thin films, were recorded respectively with a Jasco V560 spectrophotometer and a Jasco spectrofluorimeter FP750. PL-efficiency measurements on thin film (thickness of about 50 nm) were conducted using a conventional setup that consists of a 376 nm solid state laser as a light source and an integrating sphere coupled to photospectrometer (Black Comet) by Stellarnet. The experiment was controlled by an LABVIEW script that also calculated the efficiency. The setup and the calculation algorithm is the same as the one outlined in de Mello paper [29]. Maldi mass spectra were recorded in positive ion mode on a Maldi Voyager STR Applied Biosystems.

Single crystals of **B-OXA**, **FB-OXA** and **DFB-OXA** suitable for XRD analysis were obtained by sublimation. One crystal of **B-OXA** (red, $0.60 \times 0.25 \times 0.10$), one crystal of **FB-OXA** (yellow, $0.50 \times 0.05 \times 0.01$ mm) and one crystal of **DFB-OXA** (yellow, $0.60 \times 0.20 \times 0.01$ mm) were mounted at 296 K on a Bruker-Nonius KappaCCD diffractometer equipped with a graphite monochromated MoK_α radiation ($\lambda = 0.71073$ Å, CCD rotation images, thick slices, φ and ω scans to fill asymmetric unit). Semiempirical absorption correction (SADABS) was applied. The structures were solved by direct methods (SIR97 package [30]) and refined by the full matrix least-squares method on F^2 against all independent measured reflections (SHELXL program of SHELX97 package [31]). All non-hydrogen atoms were anisotropically refined. The hydrogen atoms were introduced in calculated positions and refined according to a riding model, except for H atoms on benzodifurane ring system that were found in difference Fourier maps. The final refinement converged to $R_1 = 0.0891$, $wR_2 = 0.224$ for **B-OXA**, $R_1 = 0.0613$, $wR_2 = 0.0875$ for **FB-OXA** and $R_1 = 0.0501$, $wR_2 = 0.0950$ for **DFB-OXA**. Evidences of twinning by 180° rotation around the **a** axis (twin law $1\ 0\ 0\ 0\ -1\ 0\ 0\ 0\ -1$) were found in **B-OXA**, data were not merged and refined using HKLF 5 instruction of SHELXL program. In **DFB-OXA** the Fourier maps showed a static disorder of fluorine F2 atom in two positions related by 180° rotation around C4–C7 bond (occupancy factor refined to 0.63).

CCDC-830737 (**B-OXA**), CCDC-830738 (**FB-OXA**) and CCDC-830739 (**DFB-OXA**) contain the supplementary crystallographic data for this paper. These data can be obtained free of charge at www.ccdc.cam.ac.uk/conts/retrieving.html or from the Cambridge Crystallographic Data Centre, 12 Union Road, Cambridge CB2 1EZ, UK; fax: (internet.) +44 1223/336 033.

2.2. Synthesis

2,6-Diamino-benzo[1,2-b:4,5-b']difuran-3,7-dicarboxylic acid, dibutyl ester (C4) was prepared as previously described. Amide precursors were prepared by reacting C4 with the correspondent acyl chlorides with the same procedure and the details of synthesis are reported only for the synthesis of **C4-DFB**. The benzodifuroxazinone chromophores were obtained by means of a double thermal cyclization with the reaction parameters (time and temperature) suggested by a previously performed thermo-gravimetric analysis.

2.2.1. Dibutyl 2,6-bis(2,4-difluorobenzamido)-4,8-dihydrobenzofuro[5,6-b]furan-3,7-dicarboxylate (**C4-DFB**)

C4 (0.775 g, 2 mmol) were suspended in 10 mL of dry pyridine and the system was kept under stirring at room temperature; then, 2,4-difluorobenzoylchloride (1.045 g, 5.92 mmol) was added dropwise and the previous suspension turned to a dark solution. The solution was then warmed and kept at a gentle boiling for 45 min until the formation of some precipitate was observed.

Absolute ethanol (1 mL) and after 2 min distilled water (0.2 mL) were added and the system slowly cooled down to room temperature and filtered. The yellow product was then washed in 30 mL of absolute ethanol and filtered again. The product was recrystallized by CHCl_3 /ethanol. The yield was 55%. Mp: 285 °C. ^1H NMR (CDCl_3 , 200 MHz) δ (ppm): 1.04 (t, 6H, $J = 7.4$ Hz, $-\text{CH}_3$), 1.51–1.62 (m, 4H, $-\text{CH}_2$), 1.82–1.91 (m, 4H, $-\text{CH}_2$), 4.45 (t, 4H, $J = 6.6$ Hz, $\text{O}-\text{CH}_2$), 7.56–7.64 (m, 4H, Ar–H), 7.96 (s, 2H, Ar–H), 8.07 (dd, 2H, $J_1 = 8.0$ Hz, $J_2 = 2.0$ Hz, Ar–H), 11.34 (d, 2H, $J = 13.8$ Hz, CO–NH). ^{13}C NMR (CDCl_3 , 50 MHz): δ 13.96, 19.55, 31.07, 65.26, 93.73, 103.46, 104.50, 105.05, 105.56, 113.07, 113.50, 116.87, 121.41, 134.60, 134.75, 148.96, 156.81, 158.40, 165.92. IR (KBr): 3265 (stretching N–H); 2873–2957 (stretching C–H aliphatic); 1699 (stretching C=O ester); 1601 (stretching C=O amide).

2.2.2. Dibutyl 2,6-bis(benzamido)-4,8-dihydrobenzofuro[5,6-b]furan-3,7-dicarboxylate (**C4-B**)

The synthesis was performed following the same procedure as for **C4-DFB** except that benzoyl chloride was used instead of 2,4-difluorobenzoylchloride. Yield after recrystallization was 65%. Mp: 248 °C. ^1H NMR (CDCl_3 , 200 MHz) δ (ppm): 1.04 (t, 6H, $J = 7.4$ Hz, $-\text{CH}_3$), 1.50–1.61 (m, 4H, $-\text{CH}_2$), 1.85–1.92 (m, 4H, $-\text{CH}_2$), 4.45 (t, 4H, 6.6 Hz, $\text{O}-\text{CH}_2$), 7.56–7.64 (m, 6H, Ar–H), 7.97 (s, 2H, Ar–H), 8.06 (d, 4H, $J = 8.2$ Hz, Ar–H), 11.17 (s, 2H, CO–NH). ^{13}C NMR (CDCl_3 , 50 MHz): δ 13.94, 19.55, 31.05, 65.23, 92.78, 103.34, 121.14, 127.94, 129.29, 132.82, 133.29, 148.87, 157.79, 162.88, 166.63. IR (KBr): 3268 (stretching N–H); 2874–2965 (stretching C–H aliphatic); 1706 (stretching C=O ester); 1626 (stretching C=O amide).

2.2.3. Dibutyl 2,6-bis(benzamido)-4,8-dihydrobenzofuro[5,6-b]furan-3,7-dicarboxylate (**C4-FB**)

The synthesis was performed following the same procedure as for **C4-DFB** except that 4-fluorobenzoyl chloride was used instead of 2,4-difluorobenzoylchloride. The yield was 60%. Mp: 275 °C. ^1H NMR (CDCl_3 , 200 MHz) δ (ppm): 1.05 (t, 6H, $J = 7.4$ Hz, $-\text{CH}_3$), 1.50–1.62 (m, 4H, $-\text{CH}_2$), 1.83–1.92 (m, 4H, $-\text{CH}_2$), 4.45 (t, 4H, 6.8 Hz, $\text{O}-\text{CH}_2$), 7.19–7.27 (m, 4H, Ar–H), 7.93 (s, 2H, Ar–H), 8.04–8.10 (m, 4H, Ar–H), 11.12 (s, 2H, CO–NH). ^{13}C NMR (CDCl_3 , 50 MHz): δ 13.97, 19.54, 31.05, 65.33, 92.89, 103.37, 116.29, 116.73, 121.13, 129.07, 130.45, 130.63, 148.90, 157.71, 161.75, 166.74. IR (KBr): 3281 (stretching N–H); 2876–2955 (stretching C–H aliphatic); 1712 (stretching C=O ester); 1609 (stretching C=O amide).

2.2.4. 2,8-Diphenyl-4,10-dihydro[1,3]oxazino[5''',4''',4'', 5'']furo[3'',2'':4',5']benzo-[4,5]furo-[2,3-d][1,3]oxazine-4,10-dione (**B-OXA**)

C4-B (200 mg) was placed in a petri dish in a furnace at 300 °C for 20 min. The obtained cyclized compound was then purified by sublimation. 98 mg of product was obtained for an overall yield (cyclization + sublimation) of 65%. ^1H NMR (1,1-2,2-tetrachloroethane d_2 , 200 MHz) δ (ppm): 7.58–7.68 (m, 6H, Ar–H), 8.25 (s, 2H, Ar–H), 8.45 (d, 4H, $J = 8.4$ Hz, Ar–H). IR (KBr): 1782 (C=O stretching ketone). MS: 448.03 ($\text{C}_{26}\text{H}_{12}\text{N}_2\text{O}_6$ calc. 448.07). Elemental analysis: (calc.) C 69.65 H 2.70 N 6.25, (exp.) C 69.70 H 2.64, N 6.26.

2.2.5. 2,8-Bis-(4-fluorophenyl)-4,10-dihydro[1,3]oxazino[5''', 4''',4'', 5'']furo[3'',2'':4',5']benzo-[4,5]furo-[2,3-d][1,3]oxazine-4,10-dione (**FB-OXA**)

The same procedure used for the synthesis of **B-OXA** was applied, except that the cyclization time in the furnace was 10 min. The overall yield was 70%. ^1H NMR (1,1-2,2-tetrachloroethane d_2 , 200 MHz) δ (ppm): 7.25–7.37 (m, 4H, Ar–H), 8.24 (s, 2H, Ar–H), 8.44–8.51 (m, 4H, Ar–H). IR (KBr): 1773 (C=O stretching ketone). MS: 484.06 ($\text{C}_{26}\text{H}_{10}\text{F}_2\text{N}_2\text{O}_6$, calc. 484.05). Elemental analysis: (calc.) C 64.47 H 2.08 N 5.78, (exp.) C 64.34 H 2.11 N 5.86.

2.2.6. 2,8-Bis-(2,4-difluorophenyl)-4,10-dihydro[1,3]oxazino[5''', 4''',4'', 5'']furo[3'',2'':4',5']benzo [4,5]furo-[2,3-d][1,3]oxazine-4,10-dione (**DFB-OXA**)

The same procedure used for the synthesis of **B-OXA** was applied, except that the cyclization time in the furnace was 30 min. The overall yield was 42%. ^1H NMR (1,1-2,2-tetrachloroethane d_2 , 200 MHz) δ (ppm): 7.07–7.17 (m, 4H, Ar–H), 8.24 (s, 2H, Ar–H), 8.27–8.34 (m, 4H, Ar–H). IR (KBr): 1787 (C=O stretching ketone). MS: 520.98 ($\text{C}_{26}\text{H}_8\text{F}_4\text{N}_2\text{O}_6$, calc. 520.03). Elemental analysis: (calc.) C 60.01 H 1.55 N 5.38, (exp.) C 60.14, H 1.57, N 5.37.

2.3. Computational details

Theoretical analysis of **B-OXA**, **FB-OXA** and **DFB-OXA** were performed in the framework of density functional theory (DFT).

The structural and electronic properties of the isolated molecules were computed using the NWChem package [32]. Geometry optimization, ground-state (GS) Density of States (DOS) and electronic properties were calculated using the B3LYP exchange-correlations functional combined with the 6-311G* basis set.

The GS crystal properties (band structure and DOS, in particular) were obtained using the Quantum-ESPRESSO package [33], suitable for dealing with periodic systems. We used pseudopotentials to represent the atomic cores and plane waves to expand both the electronic wave functions and charge density. The ground state properties were computed using ultrasoft pseudopotentials [34,35], with a 30 Ry and 360 Ry cut-offs for the plane-wave basis set and charge density, respectively. The GGA approximation for the exchange-correlation (XC) functional with the PBE parametrization [36] was used. The input cell parameters and atomic internal coordinates were provided by the experimental XRD analysis, described in a next section. Only the atomic internal coordinates were optimized, by computing the Hellmann–Feynmann forces until each Cartesian component of the force acting on each atom was less than 0.026 eV/Å and the total energy difference between consecutive steps less than 10^{-4} eV. Indeed, it is well known that DFT with local or semilocal XC functionals yields a poor description of interlayer interactions dominated by van der Waals (vdW) forces; yet, the weak interlayer bonding usually gives a small contribution to most of the computed properties. Using the input cell parameters usually overcomes the above cited DFT shortcoming, with good agreement with experimental data [37], with the advantage of a reasonable computational cost, that would be lost using nonlocal XC functionals, that correctly account for vdW interactions [38].

3. Results and discussion

3.1. Synthesis and chemical physical characterization

The synthetic strategy for the preparation of the benzodifurooxazinones compounds is reported in Fig. 2. The first step is the Craven reaction [39] between benzoquinone and an alkyl ester of cyanoacetic acid using NH_3 as basic catalyst to obtain a diamino-benzodifuran derivative (C_n). The latter can be reacted with benzoyl chloride, 4-fluorobenzoyl and 2,4-difluorobenzoylchloride to prepare the correspondent diamides. From the diamides it was possible to obtain the **B-OXA**, **FB-OXA** or **DFB-OXA** molecules by means of a thermally activated cyclization reaction that takes place through elimination of two molecules of alcohol.

To find the optimal temperature of cyclization we preliminarily performed an optical analysis with a thermally controlled polarized microscope: at a temperature of around 285 °C, in the molten isotropic phase of the amides, the formation of some crystalline germs occurred and at 300 °C a very fast crystallization process (assigned to the cyclization reaction), involving all the bulk, was

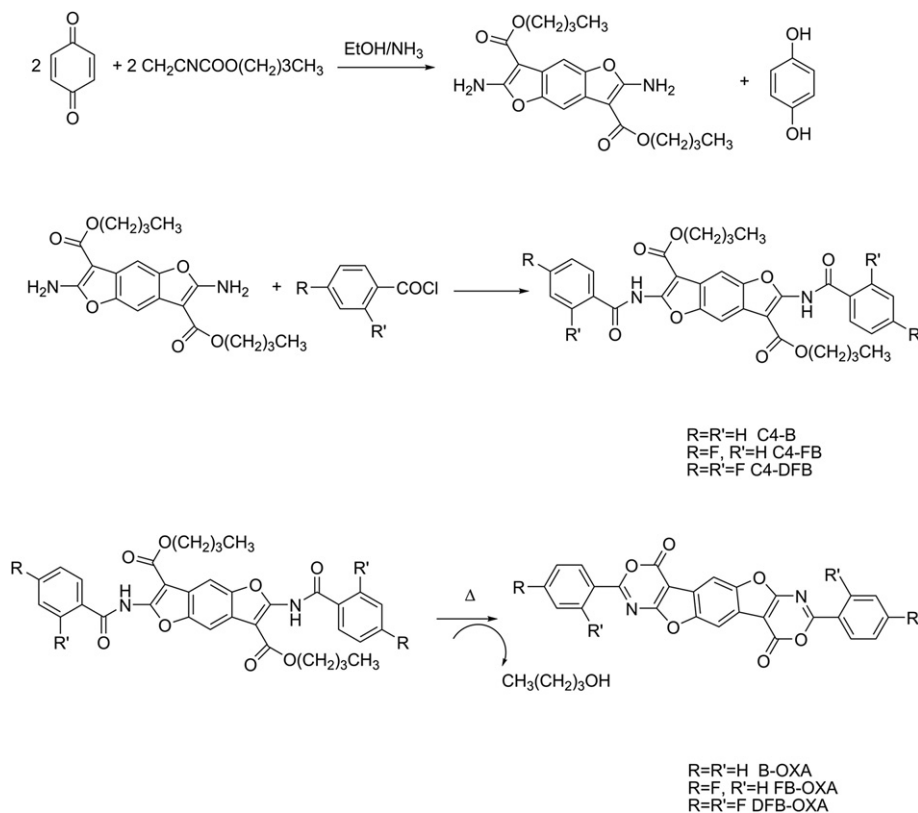


Fig. 2. Synthesis of the B-OXA, FB-OXA and DFB-OXA compounds.

observed. This process took place independently of the length of the alkyl chains of the intermediate compounds and at the same temperature: anyway, in particular in the case of the synthesis of **DFB-OXA**, the use of an intermediate amide bearing an octyl chain slowed down the crystallization process probably because of an increased solubility of **DFB-OXA** in the molten C8-DFB and a consequent reduced number of crystalline germs. To avoid long time treatment of an overheated liquid organic molecule (that could lead to undesired secondary reactions) we chose as starting amides for the synthesis of all the chromophores the butyl functionalized ones: for these derivatives in fact, the cyclization process occurred at temperatures only slightly above the melting temperature of the amides.

After this preliminary qualitative screening, we obtained more quantitative information by means of thermo-gravimetric analysis (TGA): in the thermograms of Fig. 3, the weight loss shown, as a function of time, by **C4-B**, **C4-FB** and **C4-DFB**, when placed at a constant temperature of 300 °C, is reported. In the case of the **C4-B** and **C4-DFB** compounds, the weight loss reached a plateau after, respectively, 20 and 10 min, that is consistent with the loss of two molecules of butyl alcohol and therefore with the cyclization process; for **C4-DFB** a slight negative slope was still observed even after 30 min of thermal treatment and the weight loss was higher than expected: this behaviour arises from a higher tendency to sublime of **DFB-OXA** as compared to the other two benzodifuroxazine derivatives.

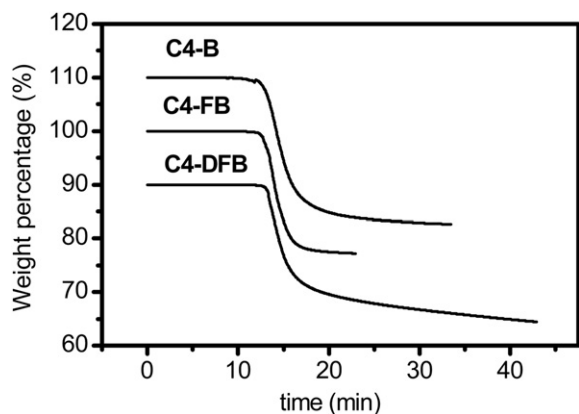


Fig. 3. Thermal cyclization of **C4-B**, **C4-FB** and **C4-DFB** at 300 °C monitored by TGA analysis. For sake of clarity **C4-B** and **C4-DFB** thermograms are translated along the Y axis (respectively +10% and 10%).

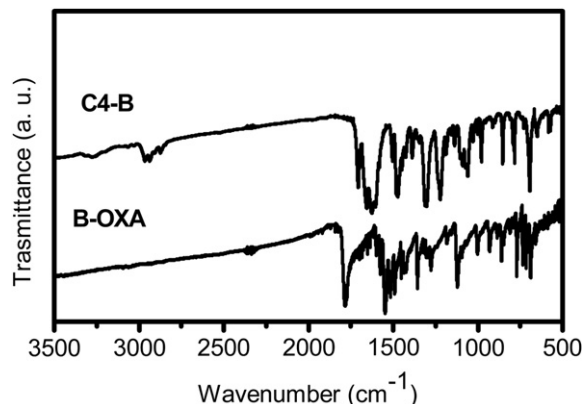


Fig. 4. FTIR spectra of **C4-B** and **B-OXA**.

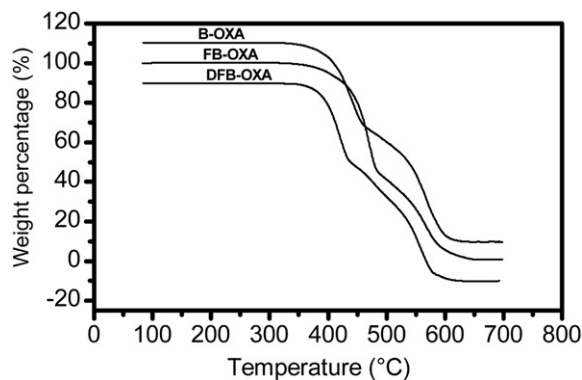


Fig. 5. Thermal stability of the **B-OXA**, **FB-OXA** and **DFB-OXA** compounds. For sake of clarity **B-OXA** and **DFB-OXA** thermograms are translated along the Y axis (respectively +10% and 10%).

Driven by the information obtained from the TGA, we quantitatively prepared the desired **B-OXA**, **FB-OXA** and **DFB-OXA** compounds by placing **C4-B**, **C4-FB** and **C4-DFB** in a furnace, pre-heated at 300 °C, for, respectively, 20, 10 and 30 min. The weight change measured after the thermal treatment of the amides **C4-B**, **C4-FB** and **C4-DFB** is, respectively, 25.0%, 23.2% and 23.7%: this weight losses are very close to the theoretical values of 24.8%, 23.4% and 22.2% expected for the formation of benzodifuroxazinone derivatives (except **C4-DFB/DFB-OXA** system in which the weight loss is higher because of the previously mentioned sublimation problems).

The compounds, which show a very poor solubility in organic solvents, were further purified by means of sublimation at atmospheric pressure in good (**B-OXA** and **FB-OXA**) or moderate (**DFB-OXA**) yield. The sublimation process, performed for sake of convenience on about 100 mg of compound, can be easily scale up to higher amount, being the sublimation performed at atmospheric pressure. The elemental analysis performed on the three compounds prepared in this way is consistent with the proposed structures shown in Fig. 1.

Both precursor amides and benzodifuroxazinone chromophores were analysed by means of FTIR spectroscopy. In the spectrum of the amides diagnostic peak are those at $\sim 3200\text{ cm}^{-1}$ (N–H stretching of the amide), around $\sim 2980\text{ cm}^{-1}$ (C–H stretching of the

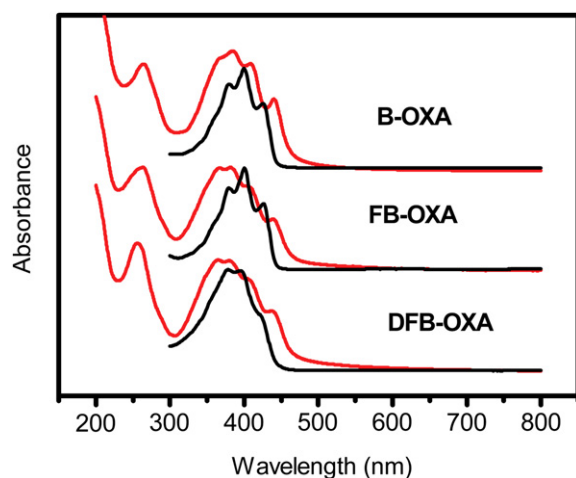


Fig. 6. UV–Vis spectra of chromophores in tetrachloroethane solution (black line) and as thin film (red line). (For interpretation of the references to colour in this figure legend, the reader is referred to the web version of this article.)

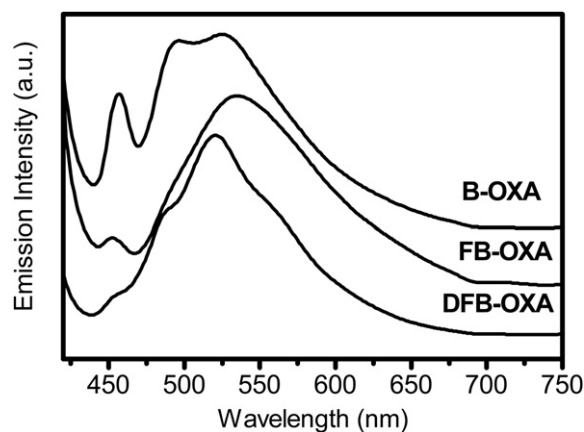


Fig. 7. Emission spectra of **B-OXA**, **FB-OXA** and **DFB-OXA** compounds.

the aliphatic chains), $\sim 1700\text{ cm}^{-1}$ (carbonyl stretching in ester), $\sim 1620\text{ cm}^{-1}$ (carbonyl stretching in amides). These signals disappeared in the spectra of the cyclized compound **B-OXA** while a new intense band at $\sim 1780\text{ cm}^{-1}$ came out, assigned to carbonyl stretching in the formed cyclic ketone. In Fig. 4, we report the spectra of **C4-B** and **B-OXA** as example.

All the intermediates and the final products have been thermally characterized by means of Differential Scanning Calorimetry (DSC) and TGA (only the final compounds). For what concerns DSC analysis on the final chromophores, neither melting or solid–solid phase transitions were observed. As previously described, TGA gave useful guidelines for the quantitative preparation of the benzodifuroxazinone chromophores. Moreover, the TGA analysis provided information about the thermal stability of the synthesized chromophores. In Fig. 5 we show the thermograms relative to weight change vs temperature of the three cyclized compounds: for **B-OXA**, **FB-OXA** and **DFB-OXA** an outstanding decomposition temperature T_d (defined as the temperature at which the weight loss is 5%) in air, respectively of 390, 402 °C and 384 °C, is observed.

Due to their very poor solubility, only a qualitative optical analysis has been carried out for **B-OXA**, **FB-OXA** and **DFB-OXA** compounds in 1,1,2,2-tetrachloroethane (TCE) solution. The UV–Vis spectra, reported in Fig. 6 (black line), show for all the chromophores an absorption maximum at around 400 nm and a clear vibronic structure.

Chromophores thin films were evaporated on quartz substrates and their UV–Vis spectra are reported in Fig. 6 (red line). Also in this case a vibronic structure (with the appearing of a new feature at higher wavelength) is observed with a general broadening and blue shift of the absorption, if compared to the behaviour shown in solution. The hypsochromic shift of the absorption in the solid state can be associated to the face-to-face packing of the molecules, characterized, as shown in the next paragraph, by a small molecular slippage along the long axis of the molecules (H aggregate).

Table 1
Optical properties of the synthesized chromophores.

Chromophores	$\lambda_{\text{abs}}^{\text{sol}}$ (nm)	$\lambda_{\text{abs}}^{\text{film}}$ (nm)	$\lambda_{\text{em}}^{\text{sol}}$ (nm)	ϕ^{sol}	$\lambda_{\text{em}}^{\text{film}}$ (nm)	ϕ^{film}
B-OXA	425/399/379	440/408/384/370	439/471/498	0.020	525	0.14
FB-OXA	426/400/380	438/406/382/366	438/470/498	0.023	521	0.15
DFB-OXA	421/395/379	437/403/379/364	439/474/495	0.011	535	0.10

^a The spectra were recorded in 1,1,2,2-tetrachloroethane solution.

^b Measurement performed in 1,1,2,2-tetrachloroethane solution using quinine sulphate as reference ($\phi_{\text{quinine sulphate}} = 0.546$ in 1 N H_2SO_4 , according to Ref. [43]).

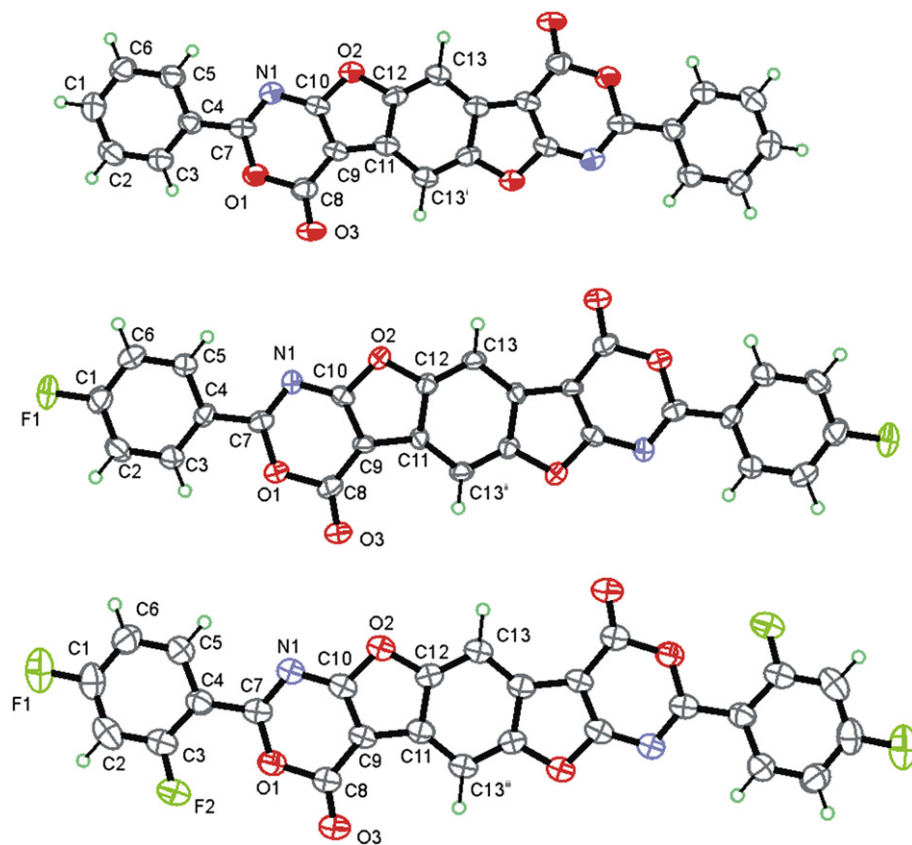


Fig. 8. Ortep view (from the top) of **B-OXA**, **FB-OXA** and **DFB-OXA**. Ellipsoids are drawn at 50% probability level ($i = -x+1, -y+1, -z$ for **B-OXA**; $ii = -x, -y, -z$ for **FB-OXA**; $iii = -x+2, -y, -z$ for **DFB-OXA**).

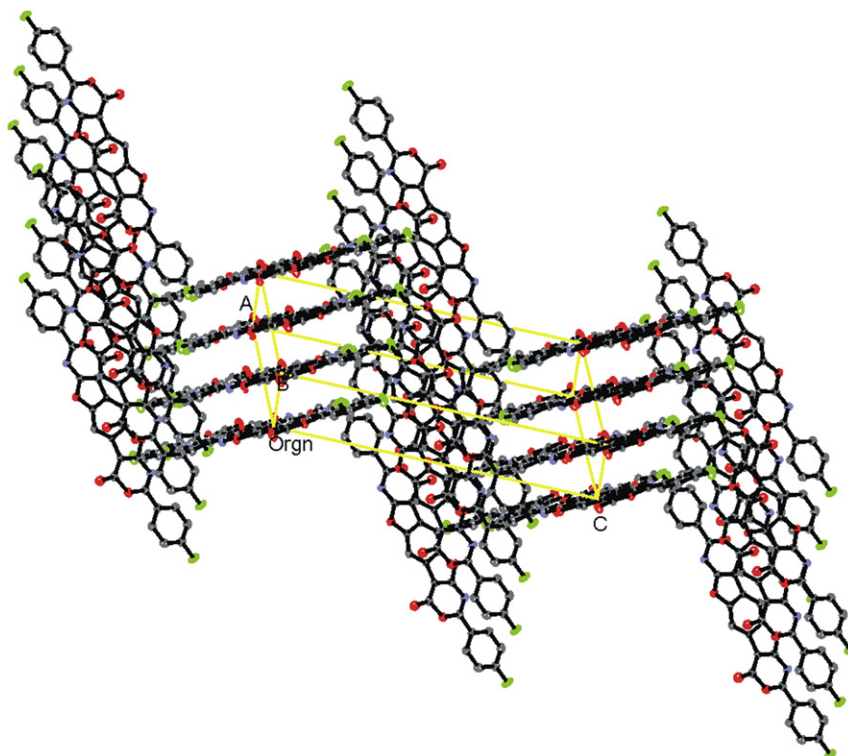


Fig. 9. Crystal packing of **FB-OXA**. H atoms are not shown for clarity.

Table 2
Pitch ($\angle P$) and roll ($\angle R$) angles and distances for **B-OXA**, **FB-OXA** and **DFB-OXA**.

	$\angle P$ (deg) ^a	$\angle R$ (deg) ^b	d (Å) ^c	d_p ^d	d_R ^e
B-OXA	59.9	25.6	3.38	5.84	1.61
FB-OXA	40.9	2.3	3.40	2.94	0.13
DFB-OXA	59.5	25.6	3.38	5.74	1.62

^a $\angle P$ is the pitch angle defined as in Ref. [22].

^b $\angle R$ is the roll angle defined as in Ref. [22].

^c π -stacking distance.

^d Displacement distance along the long molecular axis.

^e Displacement distance along the short molecular axis.

For what concerns the emission spectra, the molecules show a very low fluorescence in solution (spectra not shown), with a maximum fluorescence quantum yield ϕ of 0.23%. On the other side, in the solid state **B-OXA**, **FB-OXA** and **DFB-OXA** present a significant emission in the green zone of the spectrum (thin film

emission spectra are reported in Fig. 7), with F respectively of 14, 15 and 10%. As compared to solution, a consistent enhancement, up to 90 times, of fluorescence is observed in the solid state.

This noteworthy behaviour is rarely observed in organic compounds (where the aggregate-induced quenching of the emission is more common) and is referred to in the literature as aggregation induced emission (AIE [27,28]). In many cases, AIE is associated to a restricted motion of groups in the structure of the molecule due to the constraints of the crystalline packing: the mobility of these groups when the molecules are in diluted solution (where they can be considered as isolated molecules) are responsible for the thermal relaxation of the optical excitation and therefore the quenching of the fluorescence. In this specific case it is possible to argue that the rotation along the single bond connecting the benzodifuroxazinone core and the terminal phenyl rings, hindered in the crystalline state, is responsible for fluorescence quenching observed in solution.

Optical properties are summarized in Table 1.

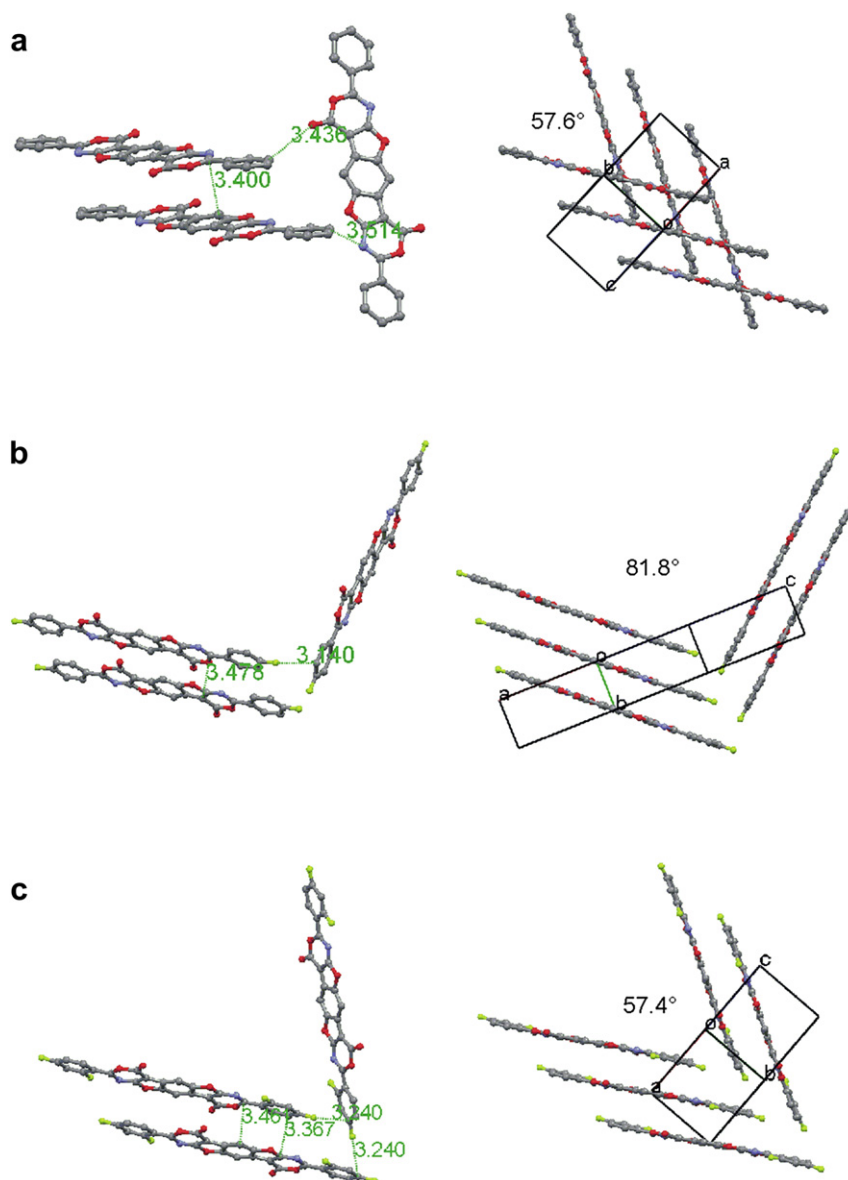


Fig. 10. Molecules (from the top) of **B-OXA**, **FB-OXA** and **DFB-OXA** showing some short intermolecular distances within a π -stack (left) and tilt of molecules in adjacent stack (right). H atoms are not shown for clarity.

Table 3

The computed HOMO and LUMO energies for the four molecules under consideration and pentacene.

Molecule	HOMO (eV)	LUMO (eV)
B-OXA	−6.05	−2.78
FB-OXA	−6.15	−2.89
DFB-OXA-O	−6.21	−2.98
DFB-OXA-N	−6.23	−3.00
Pentacene	−4.77	−2.58

3.2. Crystal structure

Single crystals of compounds **B-OXA**, **FB-OXA** and **DFB-OXA** were easily obtained by sublimation and XRD studies were performed to determine the solid state structure. The molecular structures of **B-OXA**, **FB-OXA** and **DFB-OXA** are shown in Fig. 8. Crystal data and refinement details and selected bond lengths and angles are reported, respectively, in Table S1 and S2 in Supporting information.

Each compound crystallizes in the monoclinic $P2_1/c$ space group with one half molecule (sitting on a crystallographic inversion center) contained in the asymmetric unit. All bond lengths in the three structures are normal [40]. Geometric parameters in the oxazine-4-one group agree with similar structures [41,42] and in particular the N1=C7 and C8=O3 double bonds are clearly localized.

A central planar core, consisting of five condensed rings and by two terminal phenyl rings, characterizes the molecular structure in each compound. Each terminal phenyl ring bears one *p*-attached fluorine atom in **FB-OXA** and two (*o*- and *p*-attached) fluorine atoms in **DFB-OXA**. The terminal phenyl rings are quite in-plane with the central benzodifuro-oxazin-4-one group, being stabilized in this conformation by intramolecular C–H···O and C–H···N hydrogen bonds. As a consequence, the overall shape of molecule is completely planar and fully extended.

An interesting structural feature, common to all the three compounds, concerns the crystal packing, where a π – π stacking of molecules is observed. Since a similarity in the crystal packing mode of the three compounds was found, only a view of **FB-OXA** crystal packing is reported in Fig. 9, as an example.

It turns out that the all-planar conformation of the molecules allows a π -stack structure with face-to-face molecules. This arrangement is quite different from the herringbone packing mode typical of acene-type organic semiconductors like pentacene [21]. It is to be noted that the herringbone pattern was also found in dibenzo[*d,d'*]benzo[1,2-*b:4,5-b'*]difuran [20], a compound very similar to the benzodifuroxazinone derivatives studied here, owing to the presence of the benzodifurane group and five condensed rings in the all-planar and full-extended conformation. As mentioned in the introduction, the face-to-face π -stacking in **B-OXA**, **FB-OXA** and **DFB-OXA** could positively affect the charge mobility of these compounds by allowing a better overlap of π molecular orbitals as compared to the classical herringbone structure.

Such a kind of face-to-face π -stacking arrangement in crystals may be favoured by weak intermolecular interactions. As reported previously in the literature, weak intermolecular hydrogen bonds between aryl C–H and carbonyl oxygen atom may stabilize sheets of molecules in the crystal [44]. Moreover, C–F··· π , F···H and F···F intermolecular interactions may play a role in driving the crystal packing of fluoroorganic compounds [45] and may induce a stacking of molecules with C–F bond lying parallel and above the π ring of the adjacent molecule.

These structural peculiarities are found in the crystal packing of the three structures **B-OXA**, **FB-OXA** and **DFB-OXA**. In fact, sheets of molecules are formed through intermolecular C–H···O=C weak interactions ($C2-H \cdots O3^i = 0.93, 2.585 \text{ \AA}, \angle 122.3^\circ, i = -x, 1-y, -z$ for **B-OXA**; $C2-H \cdots O3^{ii} = 0.93, 2.494 \text{ \AA}, \angle 169.2^\circ, ii = -x-1, -y+2, -z$ for **FB-OXA**; $C2-H \cdots O3^{iii} = 0.93, 2.514 \text{ \AA}, \angle 160.1^\circ, iii = 1-x, 2-y, -z$ for **DFB-OXA**). The sheets of coplanar molecules are then piled up in a slipped way to form endless columns of molecules π – π stacked along *b* axis. The interplanar distance between molecules in a π -stack is 3.38 Å for **B-OXA**, 3.40 Å for **FB-OXA** and 3.38 Å for **DFB-OXA** (the stack distance is calculated between the mean planes of adjacent molecules using Mercury program).

The criteria for a good π – π stacking can be defined by the pitch ($\angle P$) and roll ($\angle R$) angles, according to literature [22]. Small values of these angles leave a good overlap between adjacent molecules. The values calculated for the three structures are reported in Table 1.

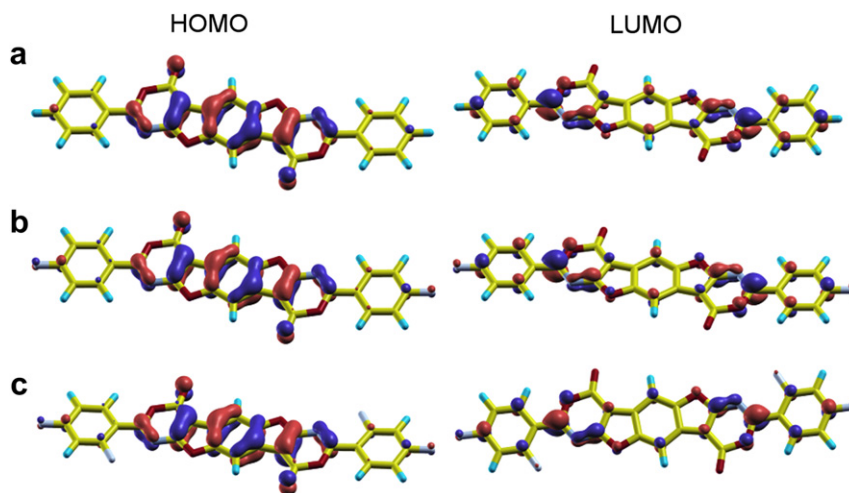


Fig. 11. The HOMO (left) and LUMO (right) wave function for the (a) **B-OXA**, (b) **FB-OXA** and (c) **DFB-OXA** molecules. Iso-surfaces are plotted for both positive (red) and negative (blue) values at a value corresponding to 10% of maximum and minimum, respectively. (For interpretation of the references to colour in this figure legend, the reader is referred to the web version of this article.)

The relatively small values observed in the Table 2 are in keep with a good π - π overlap that is a necessary condition to ensure a higher carrier mobility. In particular, the values very close to 40° and 0° for the pitch and roll angles in **FB-OXA** indicate a parallel superimposition of molecules with fluorine atom above the centroid of the adjacent stacked fluoro-aryl group.

Some short intermolecular distances are shown in Fig. 10, where it is also shown that the molecules stacked in adjacent columns are tilted at 57.6° (**B-OXA**), 81.8° (**FB-OXA**) and 57.4° (**DFB-OXA**).

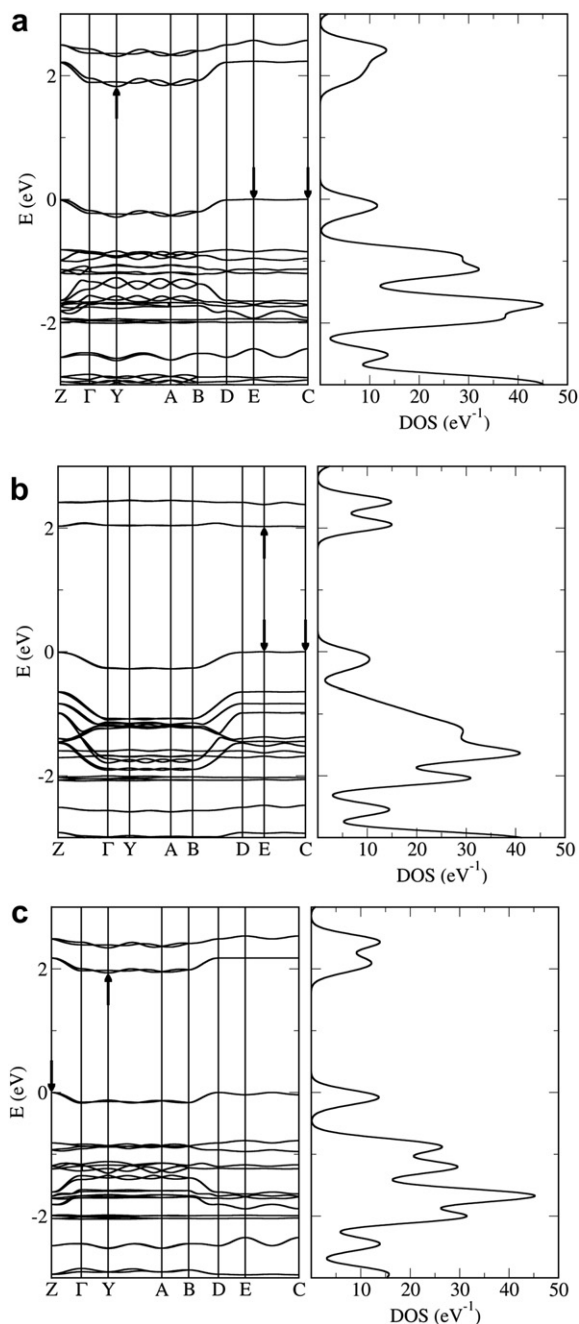


Fig. 12. The band structure (left) and DOS (right) of (a) **B-OXA**, (b) **FB-OXA** and (c) **DFB-OXA** crystal. The arrows mark the highest occupied and lowest unoccupied electronic states. DOS have been computed with a 0.15 eV Gaussian smearing. Special points in the Brillouin zone (crystal units): Z(0 ½ 0); Γ (0 0 0); Y(½ 0 0); A(-½ 0 ½); B(0 0 ½); D(0 ½ ½); E(-½ ½ ½); C(½ ½ 0). The zero energy corresponds to the top valence band.

3.3. Computational analysis

Density functional theory calculations have been performed to get insight on the electronic properties of the molecular units composing the **B-OXA**, **FB-OXA**, **DFB-OXA** crystals. It should be noticed, concerning the **DFB-OXA** molecule, that two non-equivalent configurations might be found, one (labelled as **DFB-OXA-O**) with the two additional F atoms ("F2" position in Fig. 8) facing two O atoms ("O1" positions in Fig. 8), the other (labelled as **DFB-OXA-N**) with the two additional F atoms facing the two N atoms ("N1" positions in Fig. 8).

It is interesting to have a look at the HOMO and LUMO values (at DFT level) for all the considered molecules, as shown in Table 2. The effect of fluorination stabilizes both HOMO and LUMO levels of the molecule and thus, the chromophore bandgap changes only slightly in passing from **B-OXA** to **DFB-OXA**. This behaviour is in good agreement with some results reported in previous works on fluorinated derivatives of pentacene [46] and sesquithiophene [47] (Table 3).

Moreover, the calculated HOMO energies are much lower than those calculated for pentacene and therefore a higher stability against oxidation is expected for our chromophores as compared to pentacene.

The contour plots of the HOMO and LUMO wave functions, shown in Fig. 11, do also confirm the strong similarity of the three molecules: small changes are induced by H \rightarrow F substitution (**B-OXA** \rightarrow **DFB-OXA**).

Starting from the crystallographic analysis described in the previous section, electronic structure calculations for the **B-OXA**, **FB-OXA**, **DFB-OXA** periodic crystals have been performed using the Quantum-ESPRESSO package, as described in the methodology section. The band structure and density of states (DOS) of the **B-OXA**, **FB-OXA** and **DFB-OXA** compounds are shown in Fig. 12.

Near the Fermi levels, the HOMO and LUMO complexes consist each of two bands, as the unit cell contains two molecules. Such bands show almost a dispersionless character, apart from Z- Γ and B-D paths, where a 0.2–0.3 eV dispersion is found for all the investigated crystals. Both directions correspond to 010 direction in real space hence suggesting, as expected, higher charge mobility along the π -stack directions. Parabolic fits of the valence bands near the Z point reveal band curvature corresponding to hole effective masses in the range 5–10 m_e for all crystals under consideration.

4. Conclusions

We reported on the synthesis and the properties of a new class of heteroacene molecules based on a novel benzodifuroxazinone core. The new molecules, prepared by means of a double thermal cyclization starting from precursor amides, show an outstanding thermal stability in air, with decomposition temperatures as high as 402°C . They are moreover characterized by an uncommon enhancement of fluorescent properties in the solid state, with an increase of photoluminescent quantum yield up to 90 times as compared to solution. Single crystals suitable for XRD analysis were obtained by sublimation and the crystal structure of the new compounds was solved. It turned out that the all-planar conformation of the molecules allows a π -stack structure with face-to-face molecules, stabilized by intermolecular C-H \cdots O=C weak interactions and different from the typical herringbone structure found in most of the acene derivatives. The electronic properties of the reported molecules and crystals were investigated by a detailed computational analysis: an increasing stabilization of the HOMO and LUMO energy of the molecules upon fluorination, was demonstrated. It has to be pointed out that, for all molecules, the

reported HOMO energies are much lower than the one calculated for pentacene, suggesting an increased stability toward oxidation, as expected because of the high number of heteroatoms in the structure. Finally, from the analysis of the density of states and the bandstructures of the three molecular crystals, it emerges that the charge transport is favored along one particular direction, parallel to the b-axes and π -stacking direction and holes effective masses have been calculated along this preferential direction.

All the reported properties, along with the versatility of the synthesis, that could easily be applied to design new derivatives, suggest that the new class of heteroacenes could find useful applications in the field of organic electronics.

Acknowledgements

Thanks are due to “Centro Regionale di Competenza – Nuove Tecnologie per le Attività Produttive” (CRdC-NTAP) of Regione Campania – Italy, and to “Centro Interdipartimentale di Metodologie Chimico Fisiche (CIMCF) of the University of Naples “Federico II” for X-ray facilities. The research leading to these results has received funding from the FP7/2007-2013 under grant agreement N. 264098 – MAMA.

Appendix A. Supporting information

Supplementary material associated with this article can be found, in the online version, at doi:10.1016/j.dyepig.2012.03.033.

References

- Zaumseil J, Sirringhaus H. Electron and ambipolar transport in field-effect transistors. *Chem Rev* 2007;107:1296–323.
- Facchetti A. Semiconductors for organic transistors. *Mat Today* 2007;10:28–37.
- Bao Z, Locklin J. Organic field effect transistors. Boca Raton (FL): CRC Press, Taylor & Francis Group; 2007.
- Nuyken O, Jungermann S, Viederhirn V, Bacher K, Meerholz E. Modern trends in organic light-emitting devices (OLED's). *Mon Chem* 2006;103:811–24.
- Li Z, Meng H. Organic light-emitting materials and devices. Boca Raton (FL): CRC Press, Taylor & Francis Group; 2007.
- Roviello A, Borbone F, Carella A, Diana R, Roviello G, Panunzi B, et al. High quantum yield photoluminescence of new polyamides containing oligo-PPV amino derivatives and related oligomers. *J Polymer Sci Polym Chem* 2009;47:2677–89.
- Gunes S, Neugebauer H, Sariciftci NS. Conjugated polymer based solar cells. *Chem Rev* 2007;107:1324–38.
- Thompson BC, Frechet JM. Polymer fullerene composite solar cells. *Angew Chem Int Ed* 2008;47:58–77.
- Brabec CJ, Gowrisanker S, Halls JM, Laird D, Jia S, Williams SP. Polymer fullerene bulk heterojunction solar cells. *Adv Mat* 2010;22:3839–56.
- Leenen MA, Arning V, Thiem H, Steiger J, Anselmann R. Printable electronic: flexibility for the future. *Phys Status Solidi A* 2009;206:588–97.
- Allard S, Forsters M, Souharce B, Thiem H, Scherf U. Organic semiconductors for solution processable field-effect transistors (OFET's). *Angew Chem Int Ed* 2008;47:4070–98.
- Anthony JE. Functionalized acenes and heteroacenes for organic electronics. *Chem Rev* 2006;106:5028–48.
- Facchetti A, Mushrush M, Yoon H-M, Hutchison GR, Ratner MA, Marks TJ. Buildings blocks for n type molecular and polymeric electronics. Perfluoroalkyl vs alkyl functionalized oligothiophenes (nT=2–6) Systematic of thin film microstructure, semiconductor performance and modelling of majority charge injection in field effect transistors. *J Am Chem Soc* 2004;126:13859–75.
- Jones BA, Facchetti A, Wasielewski MR, Marks TJ. Tuning orbital energetic in arylene diimide semiconductors. Materials design for ambient stability of n-type charge transport. *J Am Chem Soc* 2007;129:15259–78.
- Oh JH, Suraru SL, Lee WY, Koneman M, Hoffken HW, Roger C, et al. High performance air stable n-type organic based on core chlorinated naphthalene tetracarboxylic diimides. *Adv Funct Mat* 2010;20:2148–56.
- Facchetti A. π -Conjugated polymers for organic electronics and photovoltaic cells applications. *Chem Mat* 2011;23:733–58.
- Barra M, Biasucci M, Cassinese A, D'Angelo P, Carella A, Roviello A. Direct current and alternating current electrical transport properties of poly-[3-(4-alkoxyphenyl)thiophenes]. *J Appl Phys* 2007;102:093712.
- Yamada M, Ikemoto I, Kurada H. Photooxidation of evaporated films of polycyclic aromatic hydrocarbons studied by X-ray photoelectron spectroscopy. *Bull Chem Soc Jpn* 1988;61:1057–62.
- Li YN, Wu YL, Gardner S, Ong BS. Novel peripherally substituted indolo[3,2b]carbazoles for high mobility organic thin film transistors. *Adv Mat* 2005;17:849–53.
- Kawaguchi K, Nakano K, Nozaki K. Synthesis of ladder type p-conjugated heteroacenes via palladium catalyzed palladium N-arylation and intramolecular O-arylation. *J Org Chem* 2007;72:5119–28.
- Campbell RB, Robertson Monteath J, Trotter J. The crystal molecular structure of pentacene. *Acta Crystallogr* 1961;14:705–11.
- Curtis MD, Cao J, Kampf JW. Solid state packing of conjugated oligomers: from π -stacks to the herringbone structure. *J Am Chem Soc* 2004;126:4318–28.
- Moon H, Zeis R, Berkent EJ, Besnard C, Lovinger AJ, Siegrist T, et al. Synthesis, crystal and transistors performance of tetracene derivatives. *J Am Chem Soc* 2004;126:15322–3.
- Tannaci JF, Noji M, McBee J, Don Tolley T. 9,10-Dichlorooctafluoroanthracene as a building blocks for n-type organic semiconductors. *J Org Chem* 2007;72:5567–73.
- Anthony JE, Keaton DL, Parkin SR. A road map to stable, soluble, easily crystallized pentacene derivatives. *Org Lett* 2002;4:15–8.
- Caruso U, Panunzi B, Roviello GN, Roviello G, Tingoli M, Tuzi A. Synthesis, structure and reactivity of amino-benzodifurane derivatives. *C R Chem* 2009;12:622–34.
- Hong Y, Lan JWY, Tang BZ. Aggregation induced emission: phenomenon, mechanism and applications. *Chem Commun* 2009;113:4332–53.
- He J, Xu B, Chen F, Xia H, Li K, Ye L, et al. Aggregation induced emission in the crystals of 9,10-distyrylanthracene derivatives: the essential role of restricted intramolecular torsion. *J Phys Chem C* 2009;113:9892–9.
- de Mello JC, Wittmann HF, Friend RH. An improved experimental determination of external quantum efficiency. *Adv Mater* 1997;9:230–2.
- Altomare A, Burla MC, Camalli M, Cascarano GL, Giacovazzo C, Guagliardi A, et al. SIR97: a new tool for crystal structure determination and refinement. *J Appl Cryst* 1999;32:115–9.
- Sheldrick GM. A short history of SHELX. *Acta Crystallogr* 2008;A64:112–22.
- Valiev M, Blask EJ, Govind N, Kowalsky K, Straatsma TP, Van Dan HJJ, et al. NWChem: a comprehensive and scalable open source solution for large scale molecular simulation. *Comput Phys Commun* 2010;181:1477–89.
- Giannozzi P, Baroni S, Bonini N, Calandra M, Car R, Cavazzoni C, et al. Quantum espresso: a modular and open source software project for quantum simulations of materials. *J Phys Condens Matter* 2009;21:395502.
- Rappe AM, Rabe KM, Kaxiras E, Joannopoulos JD. Optimized pseudopotentials. *Phys Rev B* 1990;41:1227–30; Erratum in. *Phys Rev B* 1991;44:13175.
- Vanderbilt D. Soft self-consistent pseudopotentials in a generalized eigen value formalism. *Phys Rev B* 1990;41:7892–5.
- Perdew J, Burke K, Ernzerhof M. Generalized gradient approximation made simple. *Phys Rev Lett* 1996;77:3865–8.
- Mounet N, Marzari N. First principles determination of structural, vibrational and thermodynamic properties of diamond, graphite and derivatives. *Phys Rev B* 2005;71:205214.
- Rydberg H, Dion M, Jacobson N, Schroder E, Hyldgaard P, Simak SI, et al. Van der Waals density functional for layered structures. *Phys Rev Lett* 2003;91:126402.
- King TJ, Newall CE. The chemistry of colour reaction: the Craven reaction. *J Chem Soc*; 1965:974–7.
- Allen FH, Kennard O, Watson DG, Brammer L, Orpen AG, Taylor R. Tables of bond lengths determined by X-ray and neutron diffraction. Part 1. Bond lengths in organic compounds. *J Chem Soc Perkin Trans* 1987;2:S1–19.
- Kovalewsky AY, Ponomarev II. A series of three bis-2-(methyl/trifluoromethyl)-4H-3,1-benzoxazin-4-one) compounds. *Acta Crystallogr* 2000;C56:260–2.
- Thilagavathy R, Kavitha HP, Arulmozhi R, Vennila JP, Manivannan V. 2-Phenyl-4H-3,1-benzoxazin-4-one. *Acta Crystallogr* 2009;E65:o127.
- Melhuish WH. Quantum efficiencies of fluorescence of organic substances: effect of solvent and concentrations of fluorescent solute. *J Phys Chem* 1961;65:229–35.
- Sarma JARP, Desiraju G. The role of Cl...Cl and CH...O interactions in the crystal engineering of 4 Å short axis structure. *Acc Chem Res* 1986;19:222–8.
- Ribolova TV, Bagryanskaya IY. C...F, F...H and F...F intermolecular interactions and F-aggregation. Role in crystal engineering of fluoroorganic compounds. *J Struct Chem* 2009;50:741–53.
- Medina BM, Anthony JE, Gierschner J. Independent tuning of electronic levels in pentacene by site specific substitution. *ChemPhysChem* 2008;9:1519–23.
- Medina BM, Beljonne D, Egelhaaf MJ, Gierschner J. Effect of fluorination on electronic structure and optical excitation of π -conjugated molecules. *J Chem Phys* 2007;126:111101.